第三章 地震學與地球內部構造：20題重點解析

Q1. Pg、Pn、PmP 說明

- Pg（Granitic P wave）：在地殼上層（花崗岩層）中傳播的直達 P 波，速度約 5.5–6.0 km/s，為近距離（< 100 km）最先到達的震相。
- Pn（首波，Head Wave）：沿 Moho 面頂部以地函速度（約 7.8–8.2 km/s）滑行傳播的首波（head wave）。震央距超過約 180 km 後，Pn 比 Pg 更早到達，成為首波。Pn 速度直接反映上部地函最頂端的 P 波速度。
- PmP（Moho 反射波）：在 Moho 面上產生的廣角反射 P 波。在接近臨界角時，PmP 振幅極強（廣角反射），可用來精確定位 Moho 的深度與性質。

三者走時關係：近距離以 Pg 為首波；距離增大後 Pn 先到；PmP 的走時曲線介於兩者之間，為雙曲線形狀。

Q2. 如何發現 Moho 面？

1909 年克羅地亞地震學家 **莫霍洛維奇（Andrija Mohorovičić）** 分析了1909年庫帕地震的走時記錄。他觀察到：
- **兩組 P 波到時**：近距離台站只收到一組，遠距離台站則收到兩組 P 波到時。 - 他將較慢的一組（約 5.6 km/s）解釋為在地殼中傳播的直達 P 波（Pg），較快的一組（約 7.7 km/s）解釋為沿深部高速層頂端滑行的首波（Pn）。 - 利用首波走時方程 $T = x/V_1 + 2h\cos i_c/V_0$，反算出地殼厚度 **h ≈ 54 km**（後修訂為歐洲大陸約 35–40 km）。

此速度不連續面（地殼底部）即稱為 **Moho 面（莫霍面）**，標誌著地殼與地函的分界。

Q3. 全球 Moho 面的深度分布

地區	Moho 深度
大洋地殼	約 5–10 km（平均 7 km），厚度均一
大陸地殼（平均）	約 35–40 km
穩定克拉通（如東北美）	可達 42–45 km

地區	Moho 深度
山脈根部（如喜馬拉雅、安地斯）	55–70 km（地殼根，isostasy 補償）
大陸裂谷（如東非裂谷）	約 25–30 km（地殼拉薄）
北美西部（構造活躍區）	約 30 km，Pn 速度較低（熱地函）

全球 Moho 深度與地表地形呈 **負相關**（isostasy）：山越高，地殼根越深。大洋地殼的 Moho 薄且均一，反映洋中脊的均一玄武岩成因。

Q4. 什麼是 Ray Parameter（射線參數）？

射線參數 p 定義為：

$$p = \frac{\sin i}{v} = \frac{r \sin i}{v} \quad \text{（球體地球中）}$$

- i 為射線與垂直方向的夾角，v 為該點波速，r 為距地心距離。
- p 沿同一射線路徑**保持不變**（Snell 定律的推廣）。
- 幾何意義：$p = dT/d\Delta$，即走時曲線的**斜率**。
- 物理意義：p 唯一標識一條射線；p 越大，射線越接近水平出射，底轉深度越淺；p 越小，射線越陡，穿透越深。

射線參數是折射地震學和球體地球走時反演的核心概念，Herglotz–Wiechert 積分法正是以 $p(\Delta)$ 為基礎反演速度結構。

Q5. 為何遇到高速帶，某些地面接收站會收到多次到時？

當速度隨深度**急劇增加**（如地函過渡帶 410 km 或 660 km 不連續面），會產生**三叉波（Triplication）**：

- 速度急跳造成射線折射角突然改變，使得同一震央距 Δ 可有**三條不同射線**到達。
- 走時曲線出現三個分支（兩個正向 + 一個反向分支）。
- 反向分支（retrograde branch）表示 $dT/d\Delta < 0$，即距離增大，走時反而減小。
- 分支交匯處形成**焦散面（caustic）**，振幅理論上趨於無限大（實際受有限頻率限制而有大振幅）。

因此台站可依序收到：第一到時（前向分支）、焦散大振幅到時，以及反向分支到時，即**三次到時**。地函 410 km 和 660 km 不連續面正是地震學上三叉波的主要來源。

Q6. 為何遇到低速帶，某些接收站收不到波（影區）？

低速帶（Low-Velocity Zone, LVZ）中速度隨深度減小，Snell 定律要求射線向低速方向彎折：

- 射線進入低速層後**向下彎折**（而非上折回地表），沒有射線能底轉於低速層內部。
- 低速層兩側的射線底轉點出現「跳躍」——本應在低速層深度底轉的射線實際穿越低速層到更深處，導致震央距 Δ 出現跳躍。
- 跳躍對應的震央距範圍內，地表沒有任何直達射線到達，形成**影區（Shadow Zone）**。

核幔邊界（CMB）上方 P 波速度從地函的約 13.7 km/s 驟降至外核的約 8.1 km/s，就是造成 P 波在約 **98°–145°** 形成影區的原因。

Q7. 如何發現核幔邊界（Core-Mantle Boundary）？

1906 年 Oldham 首先注意到：大震央距（> 100°）時 P 波到時明顯「遲到」，推測地球內部有一個低速核。
1914 年 Gutenberg 更精確地確定 CMB 深度約為 **2900 km**，主要證據：

1. **P 波影區**：P 波在震央距 **98°–145°** 之間缺失，這正是外核低速造成射線折射入核而無法直達地表的幾何影區。
2. **PKP 波**：穿越外核的 P 波（PKP）在 145° 以後重新出現，走時曲線與地函 P 波有明顯不連續，反算出 CMB 深度。
3. **S 波消失**：外核不傳播 S 波（液態），ScS（CMB 反射 S 波）的觀測確認 CMB 為固-液邊界。
4. **PcP 反射波**：CMB 的反射 P 波 PcP 的走時精確約束 CMB 深度。

Q8. 各種體波波相介紹

體波（body wave）的命名依傳播路徑而定：

波相	說明
P	地函中直達壓縮波
S	地函中直達剪切波

波相	說明
PP / SS	在地表反射一次的 P/S 波
PPP / SSS	在地表反射兩次
PcP / ScS	在 CMB 反射的 P/S 波
PKP	穿越外核（K = 外核 P 波）的 P 波
PKS / SKP	在 CMB 轉換波相（P↔S）
PKIKP (PKP-DF)	穿越外核 + 內核的 P 波
PKiKP	在內外核邊界（ICB）反射
pP / sP	深震向上傳播、在地表反射後的 P 波（用於定震源深度）
Pdiff	沿 CMB 繞射的 P 波（影區中可觀測）
PKKP	在外核底部（ICB）反射，再回到地表

波相命名規則：大寫 P/S = 地函；K = 外核 P 波；I = 內核 P 波；J = 內核 S 波；c = CMB 反射；i = ICB 反射；小寫 p/s = 上行波（深震）。

Q9. Core Phases（核波相）介紹

核波相是穿越或在核幔邊界（CMB）/內外核邊界（ICB）相互作用的震相：

PKP 波（穿越外核 P 波）：
- 走時曲線有兩個分支：**AB 分支**（反向，高 p）和 **BC 分支**（正向，低 p），在約 143° 匯合形成焦散（大振幅）。
- **PKIKP（DF 分支）**穿越固態內核，在影區（98°–143°）中可見，是研究內核的主要震相。

Pdiff：當射線參數恰好使射線沿 CMB 滑行，形成繞射波，可在影區中觀測到，但振幅小且頻率低。

PKP precursors（PKP 前兆波）：PKP-AB 波在下部地函或 CMB 附近散射體上散射，提早進入影區，是研究 CMB 附近小尺度不均勻性的工具。

ScS / PcP：CMB 反射波，ScS 的 SH 分量在 CMB 完全反射（液態外核不傳 S 波），記錄清晰；PcP 的阻抗差僅約 5%，較弱。

SKS / PKS：穿越外核時 S 轉 P（或 P 轉 S），因通過液態外核，SKS 無各向異性影響，僅在穿越上部地函時發生剪切波分裂，是研究地函各向異性的理想波相（見 Q14）。

Q10. 什麼是 Antipodal Focusing？

對蹠點聚焦（Antipodal Focusing）指地震波在傳播至震源**對蹠點**（震央距 $\Delta = 180°$）附近時，能量從各方向匯聚集中的現象：

- 球體地球的對稱性使得從震源出發的所有方位角的射線，在穿越地球後都聚焦至對蹠點附近。
- 幾何擴散因子 $\propto 1/\sin\Delta$ 在 $\Delta \to 180°$ 時趨向無窮（類似 $\Delta = 0°$ 震源附近），造成振幅理論上極大。
- 實際上，速度結構的橫向不均勻性使聚焦點偏離理想對蹠點，但仍可觀測到顯著的**振幅增強**。
- 面波的幾何擴散因子 $\propto 1/\sin\Delta$ 在 $\Delta = 0°$ 和 $180°$ 處最大（能量集中），在 $90°$ 最小。

Q11. Upper Mantle Structure：低速帶與高速帶說明

上部地函速度結構由上而下：

岩石圈（Lid）：地殼下方至約 80–200 km，P 波速度高（~8.1 km/s），剛性強，隨板塊運動，厚度因地而異（洋中脊 < 10 km，穩定克拉通 ~200 km）。

低速帶（LVZ, Low-Velocity Zone）：約 80–220 km 深度，速度比 Lid 低，原因： - 溫度接近岩石熔點，部分礦物開始軟化甚至部分熔融。 - 含有微量流體或熔融相，降低了彈性模量。 - 力學上對應**軟流圈（Asthenosphere）**，驅動板塊運動。 - 大洋板塊下 LVZ 明顯，穩定克拉通下 LVZ 可能不存在。

高速帶（高速不連續面）： - **410 km 不連續面**：橄欖石 → 尖晶石相變，速度急升，產生三叉波。 - **660 km 不連續面**：尖晶石 → 鈣鈦礦 + 鎂方鐵礦相變，速度再次急升，另一組三叉波。 - 這兩個不連續面界定了**地函過渡帶（Transition Zone）**。

660 km 以下為**下部地函**，速度平滑上升至 CMB 上方的 D″層。

Q12. Anisotropic Earth Structure（各向異性地球構造）說明

地球並非完全各向同性，速度因方向不同而變化：

成因機制： 1. **LPO（晶格優選方向）**：橄欖石（上部地函主要礦物）在剪切應力下晶軸定向排列，快速軸沿板塊運動方向。 2. **SPO（形狀優選方向）**：交替岩層（如薄岩漿層與固態岩層）整體呈各向異性。

橫向各向同性（Transverse Isotropy）：對稱軸垂直（如水平岩層），需 5 個彈性常數（A, C, F, L, N）。Love 波與 Rayleigh 波測得的剪切速度差（$V_{SH} > V_{SV}$）正是上部地函橫向各向同性的證據。

方位各向異性：Pn 波速隨方位角呈 $\cos 2\theta$ 變化，在洋底擴張脊附近最明顯（橄欖石快速軸沿擴張方向）。

內核各向異性：PKIKP 沿極方向比赤道方向快約 3%，解釋為鐵晶體沿自轉軸優選排列。

Q13. 剪切波分裂（Shear Wave Splitting）說明

剪切波分裂（Shear Wave Splitting）發生於 S 波進入各向異性介質時：

1. 原始 S 波分裂為**兩個正交極化的 S 波**：快 S 波（S_1，沿快速軸極化）和慢 S 波（S_2，沿慢速軸極化）。
2. 兩波以不同速度傳播，到達台站時產生**時間延遲** δt（秒）。
3. 測量參數：**快波極化方向** ϕ（反映各向異性對稱軸方向）和**延遲時間** δt（反映各向異性強度 × 厚度）。

地質意義： - 上部地函 δt 通常為 0.5–2 秒，快波方向常與板塊絕對運動方向一致。 - 隱沒帶中，慢軸可能平行海溝（橄欖石 B 型組構）。 - 下地殼（片麻岩層理）和 D″層也可造成分裂。

Q14. 為何使用 SKS 波相研究剪切波分裂？

SKS 波相（S → 外核 P → 地函 S）是研究上部地函各向異性的最佳震相，原因：

1. **外核清除記憶**：SKS 在外核以 P 波傳播（液態外核無 S 波），到達 CMB 再轉換為 S 波時，**原始震源端的各向異性資訊被抹除**，所觀測到的分裂 100% 來自接收台站下方的地函。
2. **近垂直入射**：SKS 以近垂直角度穿越上部地函，傳播路徑集中於台站正下方，空間解析度高。

3. **SH/SV 分量清晰**：SKS 理論上為純 SV 極化，若地震記錄的橫向（SH）分量上出現 SKS 能量，即為各向異性分裂的直接證據。
4. **大震央距可用**：SKS 在 84°–180° 均可觀測，資料豐富。

Q15. 解釋圖 3.6-1 與 3.6-7

For an isotropic material, the c_{ijkl} tensor can be written in terms of two independent elastic constants

$$c_{ijkl} = \lambda\delta_{ij}\delta_{kl} + \mu(\delta_{ik}\delta_{jl} + \delta_{il}\delta_{jk}), \tag{3}$$

so its matrix form is

$$C_{mn} = \begin{pmatrix} \lambda+2\mu & \lambda & \lambda & 0 & 0 & 0 \\ \lambda & \lambda+2\mu & \lambda & 0 & 0 & 0 \\ \lambda & \lambda & \lambda+2\mu & 0 & 0 & 0 \\ 0 & 0 & 0 & \mu & 0 & 0 \\ 0 & 0 & 0 & 0 & \mu & 0 \\ 0 & 0 & 0 & 0 & 0 & \mu \end{pmatrix}. \tag{4}$$

However, the crystal structures of many earth materials require additional independent elastic coefficients. For example, ice, quartz, olivine, or plagioclase feldspar require 5, 6, 9, and 21 constants, respectively. In such cases, the matrix is more complicated.

One of the most important forms of anisotropy, known as *transverse isotropy* (also known as radial anisotropy, axisymmetry, and cylindrical symmetry), occurs for a stack of layered materials. Each layer is isotropic in its properties, but these properties differ between layers (as in plywood). Thus the elastic properties, and hence seismic velocities, of the stack as a whole are identical regardless of the amount of rotation about the axis of symmetry, which is perpendicular to the layers. However, these aggregate properties differ in the perpendicular directions.

A transversely isotropic material can be characterized by five independent elastic coefficients, A, C, F, L, N, that represent its aggregate properties. If the axis of symmetry is x_3, so properties in that direction differ from those in the x_1–x_2 plane, the elastic constant matrix (Eqn 4) becomes

$$C_{mn} = \begin{pmatrix} A & A-2N & F & 0 & 0 & 0 \\ A-2N & A & F & 0 & 0 & 0 \\ F & F & C & 0 & 0 & 0 \\ 0 & 0 & 0 & L & 0 & 0 \\ 0 & 0 & 0 & 0 & L & 0 \\ 0 & 0 & 0 & 0 & 0 & N \end{pmatrix}. \tag{5}$$

Comparisons with matrices 2 and 4 show that terms that were the same for an isotropic material (consider C_{11} and C_{33}, or C_{55} and C_{66}) now differ, because terms involving the x_3 direction differ from those in the x_1 or x_2 directions.

This matrix gives the velocities of waves propagating in different directions. First, consider waves propagating in the x_1 direction (Fig. 3.6-2, *top*). By analogy to the isotropic case, A corresponds to $\lambda + 2\mu$ for the x_1 direction, N corresponds to μ for the x_2 direction, and L corresponds to μ for the x_3 direction. Thus the P velocity and the two orthogonal S velocities are

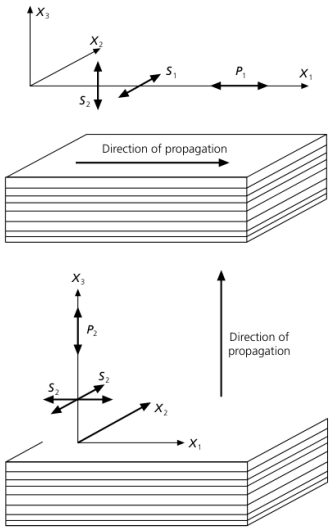

Fig. 3.6-2 Cartoon showing the effects of transverse isotropy due to layering. *Top*: Directions of oscillations for *P* and *S* waves propagating in the x_1 direction, in the plane of layering. The shear wave oscillating in the plane of the layering has velocity S_1, which is generally faster than that for the shear wave oscillating across the layers, S_2. *Bottom*: Directions of oscillations for *P* and *S* waves propagating in the x_3 direction, perpendicular to the layering. The compressional wave velocity, P_2, is generally less than P_1. Both shear waves have the same velocity, S_1.

$$P_1 = (A/\rho)^{1/2}, \quad S_1 = (N/\rho)^{1/2}, \quad S_2 = (L/\rho)^{1/2}. \tag{6}$$

Hence the velocity of shear waves traveling in this direction depends on the directions of their particle motions. The waves become split, with waves polarized in one plane traveling faster than those polarized in the other. This is one way to get splitting like that shown in Fig. 3.6-1. These results would be the same for propagation in the x_2 direction, or any other direction in the x_1–x_2 plane, because physical properties in this plane are independent of direction.

In many applications, the horizontally layered earth shows transverse isotropy about a vertical axis. The *SH*-wave velocity S_1 is generally faster than the *SV* velocity S_2, because the *SH* displacement is preferentially in the fast layers, whereas *SV* samples both equally. An interesting consequence is that the shear velocity inferred from the dispersion of Love waves, which are *SH* waves, would be higher than that from Rayleigh waves, which involve *SV*.

圖 3.6-1（橄欖石晶體各向異性示意圖）：
展示橄欖石單晶的三個主軸（a, b, c 軸）對應不同的 P 波速度。沿 a 軸方向（[100]）最快（~9.89 km/s），沿 b 軸（[010]）居中，沿 c 軸（[001]）最慢（~7.72 km/s）。整體各向

異性度 k ≈ 25%。說明上部地函的 LPO 如何造成 P 波速度的方向依賴性，若橄欖石 a 軸沿板塊運動方向排列，則 Pn 在板塊運動方向最快。

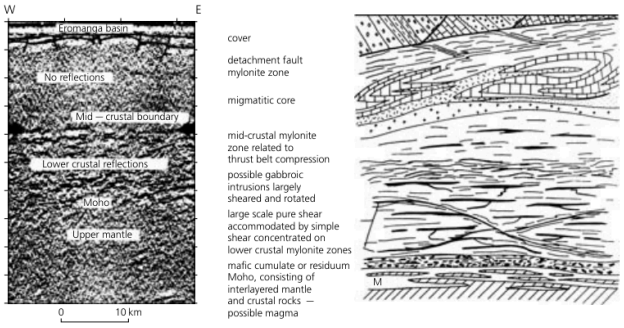

Fig. 3.6-5 *Left*: Seismic reflection profile of the crust and upper mantle in eastern Australia. The lower crust has multiple, discontinuous, and sub-horizontal reflectors possibly due to strain-induced fabrics, igneous layering, or free fluids. This structure yields vertical-axis transverse isotropy. (Finlayson *et al.*, 1989. *Properties and Processes of Earth's Lower Crust*, 1–16, by permission of Australian Geological Survey Organisation.) *Right*: Schematic cross-section of the crust in the northern Ruby Mountains of the North American Basin and Range. There is a strong tendency toward horizontally layered features, although the likely origins of such fabrics vary with depth. (Smithson, 1989. *Properties and Processes of Earth's Lower Crust*, 53–63, permission as above.)

(Fig. 3.6-4, *top*) appear to orient olivine crystals preferentially in the spreading direction, along their [100] slip axes.[1] Because *P* waves propagate fastest in this direction (Fig. 3.6-3), P_n head waves that sample the uppermost mantle just below the Moho (Section 3.2.1) show a strong azimuthal velocity dependence (Fig. 3.6-4, *bottom*). This variation is approximately described by the cos 2θ term in Eqn 9, where θ is measured from the spreading direction, so the velocity is highest in the spreading direction or 180° from it. This anisotropy is "frozen in" as the lithosphere ages, and so records the spreading direction.

Because continental crust is more complicated than oceanic crust, so is its anisotropy. A primary source of anisotropy in the upper crust is the presence of cracks, often fluid-filled. Such cracks often have a near-vertical orientation induced by regional stress fields parallel to the cracks. When these cracks occur in horizontal sediments that would by themselves have vertical-axis transverse isotropy, the combined result can be orthorhombic symmetry. The lower continental crust tends to have strong sub-horizontal layering, perhaps resulting from ductile deformation, which causes seismic anisotropy. Figure 3.6-5 shows such layering in a seismic reflection profile and a schematic diagram.

Anisotropy within and beneath continental lithosphere is often studied with a technique called *shear wave splitting*. When *SKS* waves convert from *P* waves in the outer core to *S* waves in the lower mantle, they are entirely polarized in the radial (*SV*) direction, because all the initial *SH* energy was reflected when the downgoing *S* wave encountered the core–mantle boundary. As these shear waves travel across the mantle and crust, however, they can be *split* when traveling through anisotropic media (Fig. 3.6-6). Assuming transverse isotropy with a horizontal axis of symmetry, the two polarized waves travel at different

[1] This representation of crystallographic axes is discussed in mineralogy texts like Klein and Hurlbut (1985).

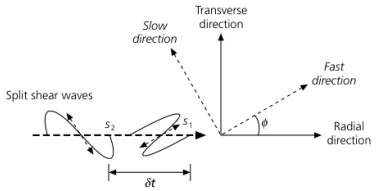

Fig 3.6-6 Splitting of an incoming shear wave into pulses oriented along the fast (s_1) and slow (s_2) directions of anisotropy. The polarization angle ϕ gives the rotation of the fast axis relative to the radial propagation direction, and δt is the time difference between the split pulses.

speeds and arrive at different times. Thus, if the *SKS* signal on the radial component in an isotropic earth is $s(t)$, its projection into the fast and slow polarizations is, respectively,

$$s_1(t) = s(t)\cos\phi, \quad -s_2(t) = s(t-\delta t)\sin\phi, \tag{12}$$

where ϕ is the polarization angle between the radial direction and the fast axis, and δt is the delay time between the fast and slow polarizations. We would normally not expect any *SKS* on the transverse component, but anisotropy yields a combination of both the fast and the slow polarizations on both the radial and the transverse components, given by

$$R(t) = s(t)\cos^2\phi + s(t-\delta t)\sin^2\phi,$$
$$T(t) = [(s(t) - s(t-\delta t))/2]\sin 2\phi. \tag{13}$$

For example, in Fig. 3.6-7a (*top*), *SKS* appears on the transverse component. The two components are rotated to yield the fast and slow polarizations, $s_1(t)$ and $s_2(t)$ (Fig. 3.6-7a, *middle*). The time shift δt is then applied, and the signals are rotated

圖 3.6-7（全球 SKS 分裂觀測圖）：

世界地圖上以短線段標示各台站測得的 SKS 快波方向與延遲時間（線段長度代表 δt，方向代表 ϕ）。主要特徵： - 大多數大陸台站快波方向與**板塊絕對運動方向**一致，支持地函流動控制橄欖石定向的觀點。 - 隱沒帶附近可見快波方向與海溝平行或垂直，反映不同的橄欖石組構型態。 - 穩定克拉通（如北美克拉通）的 δt 較小，反映較弱的各向異性或凍結的古構造各向異性。

Q16. 波傳遞時能量如何衰減？

地震波振幅衰減有四種機制：

1. **幾何擴散（Geometric Spreading）**：波前面積隨距離增大，能量密度降低。體波振幅 $\propto 1/r$（球面波前面積 $\propto r^2$）；面波振幅 $\propto 1/\sqrt{r}$（柱面擴散）。

2. **散射（Scattering）**：速度不均勻體（尺度接近波長）將能量散射至其他方向，形成主波後的**尾波（coda）**，主波振幅降低。

3. **多路徑（Multipathing）**：橫向速度不均勻使射線發散（散焦）或聚焦，造成振幅的空間不均一，但不損耗總能量。

4. **非彈性衰減（Anelastic/Intrinsic Attenuation）**：地震波動能轉化為熱能，以**品質因子 Q** 量化：
   $$A(x) = A_0 \exp!\left(-\frac{\omega x}{2cQ}\right)$$
   高頻衰減更快（ω 大）；Q 越小，衰減越嚴重。衰減對溫度呈**指數依賴**，是探測深部熱異常的敏感指標。

Q17. 解釋圖 3.7-1

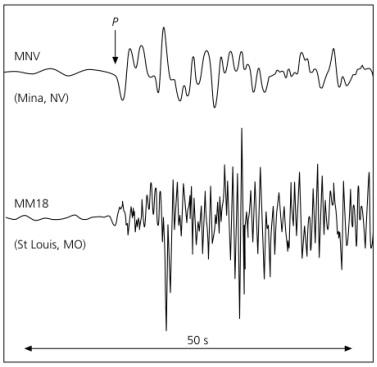

Fig. 3.7-1 Regional variations in attenuation seen in seismograms from an April 14, 1995, earthquake in Texas recorded in Nevada (MNV, $\Delta = 15°$) and Missouri (MM18, $\Delta = 14°$). The MNV record has less high frequency energy because the tectonically active western USA is more attenuating than the stable mid-continent.

there are many important implications and applications of anelasticity.

Anelasticity results because the kinetic energy of elastic wave motion is lost to heat by permanent deformation of the medium. The large-scale, or macroscopic, term for this process is *internal friction*. Among the smaller-scale, or microscopic, mechanisms that may cause this dissipation are stress-induced migration of defects in minerals, frictional sliding on crystal grain boundaries, vibration of dislocations, and the flow of hydrous fluids or magma through grain boundaries. Theoretical and experimental work is being carried out to examine possible mechanisms of seismic attenuation.

The study of anelasticity has lagged behind that of the elastic wave velocities because of the complexities involved in measuring attenuation and understanding its physical causes. Although measuring seismic wave amplitudes is straightforward, they depend on both the source, which is not perfectly known, and all the elastic and anelastic effects anywhere along the paths that the seismic energy traveled between the source and the receiver. Hence it can be hard to distinguish the effects of anelasticity from elastic processes.

This inherent uncertainty is somewhat compensated by the fact that variations in anelasticity are large, as illustrated by comparison of records of an earthquake in Texas at stations in Nevada and Missouri (Fig. 3.7-1). The Nevada seismogram has much less high-frequency energy, showing that the crust in the western USA is much more attenuating than that in the Midwest. By comparison, seismic velocity variations between these areas are generally less than ±10%. Even so, because of the difficulties in measuring attenuation, variations in attenuation at both regional and global scales are much less resolved than similar variations in velocity.

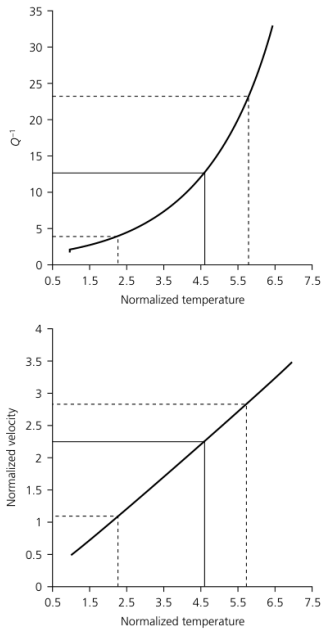

Fig. 3.7-2 Schematic representation of the variations of seismic attenuation (*top*) and normalized velocity (*bottom*) as a function of normalized temperature changes. Attenuation is more sensitive to increased temperature. (Romanowicz, 1995. *J. Geophys. Res., 100*, 12,375–94, copyright by the American Geophysical Union.)

Attenuation is valuable for studying temperature variations within the earth. Many important geophysical processes (mantle convection, plate tectonics, magmatism, etc.) involve lateral variations in temperature. Elastic velocities are also sensitive to temperature, but are better for mapping cold (fast) anomalies like subducting slabs than hot (slow) material like that at midocean ridges (Section 2.5.10). As shown in Fig. 3.7-2, seismic velocities depend nearly linearly upon temperature, whereas attenuation depends exponentially on temperature. Thus combining velocity and attenuation studies can provide valuable information. Figure 3.7-3 shows the velocity and attenuation structure at a portion of the East Pacific rise axis, where a low-velocity, high-attenuation region is interpreted as a melt-filled magma chamber.

圖 3.7-1（地震波振幅衰減與幾何擴散示意圖）：

展示球面波前從震源向外擴展的示意。隨震央距增大，波前面積 $\propto r^2$ 增大，但能量守恆使單位面積能量密度 $\propto 1/r^2$ 降低，振幅 $\propto 1/r$ 衰減。圖中同時標示：- 在 $\Delta = 90°$ 處，面波幾何擴散因子最大（能量最分散）。 - 在 $\Delta = 0°$ 和 $180°$（震源與對蹠點）處，幾何擴散因子趨向最小（能量聚焦）。 此圖說明幾何擴散是振幅衰減的第一階效應，也是計算震源強度（地震規模）時必須校正的項目。

Q18. 解釋圖 3.7-5

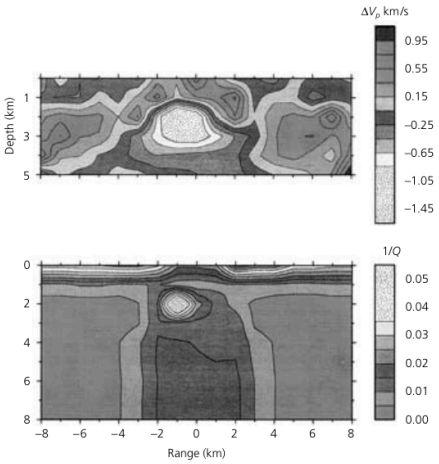

Fig. 3.7-3 Results of *P*-wave velocity (*top*) and attenuation (*bottom*) tomography across the axis of the East Pacific rise. (Solomon and Toomey, 1992, reproduced with the permission of Annual Reviews Inc.)

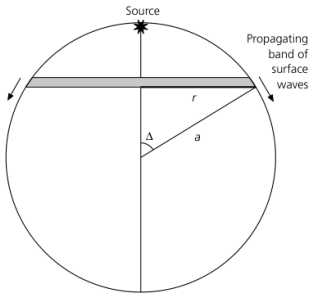

Fig. 3.7-4 Geometric spreading of surface waves for a laterally homogeneous earth yields a wave front that is a ring whose circumference varies as $a \sin \Delta$.

3.7.2 *Geometric spreading*

The most obvious effect causing seismic wave amplitudes to vary with distance is geometric spreading, in which the energy per unit wave front varies as a wave front expands or contracts. Geometric spreading differs for surface and body waves. For a homogeneous elastic spherical earth, a surface wave front would spread as it moved from the source to a distance 90° away, refocus as it approached the antipode on the other side of the earth from the source, and so on. The amplitudes would be largest at the source and antipode, where all the energy would be concentrated, and smallest halfway between, 90° from the source. On a homogeneous flat earth, the surface waves would spread out in a growing ring with circumference $2\pi r$, where r is the distance from the source. Conservation of energy[2] requires that the energy per unit wave front decrease as $1/r$, whereas the amplitudes, which are proportional to the square root of energy (Eqn 2.4.65), decrease as $1/\sqrt{r}$. However, because the earth is a sphere, the ring wraps around the globe (Fig. 3.7-4), making the energy per unit wavefront vary as

$$1/r = 1/(a \sin \Delta), \quad (1)$$

where Δ is the angular distance from the source. Thus the amplitudes decrease as $(a \sin \Delta)^{-1/2}$, with minimum at $\Delta = 90°$, and maxima at 0° and 180°. Actually, not all the energy would focus at the antipode and source even if the earth had no lateral variations in velocity, because some defocusing would result from the earth's ellipsoidal shape. Lateral heterogeneity, discussed next, further distorts the wavefront.

For body waves, consider a spherical wavefront moving away from a deep earthquake. Energy is conserved on the expanding spherical wavefront whose area is $4\pi r^2$, where r is the radius of the wavefront. Thus the energy per unit wave front decays as $1/r^2$, and the amplitude decreases as $1/r$. In reality, because body waves travel through an inhomogeneous earth, their amplitude depends on the focusing and defocusing of rays by the velocity structure. The effects of the variations in velocity with depth were shown in Section 3.4 by considering the density of rays with different incidence angles that arrive at a given distance. These amplitude variations are viewed as geometric spreading and described by the second derivative of the travel time curve (Eqn 3.4.20). Thus, although the phenomenon of geometric spreading is intuitive, quantification of its effects is complicated.

3.7.3 *Multipathing*

Seismic waves are also focused and defocused by lateral variations in velocity. Although physically this process is the same as the effects of vertical variations, it is often distinguished by the term *multipathing*. The distinction reflects our view of the earth as an essentially layered planet with secondary lateral variations.

As we discussed for tsunamis (Fig. 2.8-9), seismic waves refract towards low-velocity anomalies and away from high-velocity anomalies. Figure 3.7-5 illustrates this effect for a plane wave passing through a refracting layer of variable thickness.

[2] As we saw in discussing wave reflection and transmission (Section 2.2.4), amplitudes are easier to visualize, but energy is conserved, and hence often more useful for understanding wave behavior.

圖 3.7-5（Q 值對波形頻率成分影響圖）：

展示同一地震在不同震央距台站記錄的波形（或同一台站不同頻率分量）。隨距離增大：- **高頻成分衰減較快**（$e^{-\omega t/2Q}$ 中 ω 大），遠距離波形頻率成分明顯偏低頻。- 波形脈衝**展寬（pulse broadening）**：高頻丟失使波形變寬、振幅峰值降低。- 比較不同路徑（如穿越熱弧後盆地 vs. 冷板片）的波形，可定量估計路徑積分衰減（$t^*= \int ds/(vQ)$），進而反演 Q 的三維結構。

Q19. 解釋圖 3.7-10

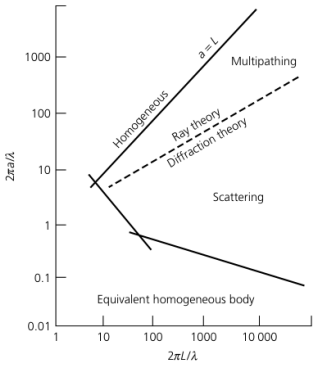

Fig. 3.7-8 Schematic representation of different approaches to seismic wave propagation in a medium with velocity heterogeneity. The approach depends on the ratio of the heterogeneity size a to the wavelength λ and the distance L the wave travels through the heterogeneous region. (After Aki and Richards, 1980. From *Quantitative Seismology*, © 1980 by W. H. Freeman and Company, used with permission.)

3.7.4 *Scattering*

A related effect to multipathing is the scattering of seismic waves. Both effects are complicated, and the distinction between them is gradational. As shown in Fig. 3.7-8, whether the effects of velocity heterogeneity are regarded as scattering depends on the ratio of the heterogeneity size to the wavelength and the distance the wave travels through the heterogeneous region. When the heterogeneity is large compared to the wavelength, we regard the wave as following a distinct ray path that is distorted by multipathing. When the velocity heterogeneities are closer in size to the wavelength, we think of scattered energy rather than distinct ray paths. However, when the heterogeneities are much smaller than the wavelength, they simply change the medium's overall properties. The further the wave travels in the heterogeneous region, the more useful the scattering description becomes. Hence for longer distances, the wavelength range viewed as scattering increases.[3]

Figure 3.7-8 also illustrates that diffraction can be viewed as behavior intermediate between scattering and multipathing.

As we have seen, some of the behavior of diffracted waves can be derived either using a Huygens' source scattering representation (Section 2.5.10) or by using ray paths in a medium with variable velocity, as for the head wave (Section 3.2.1) or core diffraction (Section 3.5.2). These ray paths were not truly geometric, in that energy was required to follow paths that did not obey Snell's law. The distinction between ray theory and diffraction depends on wavelength, as discussed in Section 2.5.10, so waves diffracted around the core are depleted in the higher frequencies.[4]

Scattering can be viewed in different ways. In some situations we view the scattering as deterministic, and try to image distinct scatterers. For example, migration methods in reflection seismology (Section 3.3.7) seek to undo the effects of scattering and produce a clearer image of the subsurface. In other situations, we view the medium as containing many scatterers and consider their effects on the wave field statistically. This approach is taken to the scattering of *PKP* waves (Fig. 3.5-8), with a wavelength of about 10 km, by lower mantle heterogeneities of about that size.

Scattering is especially important in the continental crust, which has many small layers and reflectors resulting from billions of years of continental evolution. Although these structures do not significantly affect waves with wavelengths longer than tens of km, for shorter-wavelength waves they can act as point scatterers or Huygens' sources. Hence some of the scattered energy arrives at a receiver after the initial pulse that obeyed Fermat's principle and took the shortest path. This scattered energy causes an arrival to have a *coda*, a tail of incoherent energy that decays over a duration of seconds or minutes. The main arrival has a polarity related to the direction of propagation that can be observed on a three-component seismometer by forming particle motion plots (Fig. 2.7-6). By contrast, the scattered energy arrives from various directions and thus shows little or no preferred particle motion.

Figure 3.7-9 demonstrates the scattering for a seismic arrival. The unscattered wave travels the shortest distance and gives the initial arrival (*left*). Scattered energy lost from this arrival that instead arrives later could have been scattered from an infinite number of locations that would yield the observed travel time. In a constant-velocity medium, the locus of these possible scatterers forms an ellipsoid with the source and the receiver as foci (*center*). Larger ellipsoids define the possible scatterers for energy that arrives later (*right*). These ellipsoids are distorted by velocity heterogeneity and are analogous to the Fresnel volume used when we consider the waves as following distinct ray paths.

Scattering is especially noticeable on the moon. Figure 3.7-10 contrasts seismic records of an earthquake and the impact of a rocket on the moon. Most of the earthquake's energy arrives in the main *P*- and *S*-wave arrivals. By contrast, on the moon

[3] The fact that light scattering in the atmosphere depends on wavelength and the distance traveled has familiar consequences. Because the shortest wavelengths of visible light are the most scattered, blue light reaching us from all directions makes the sky appear blue. The loss of blue light makes the sun appear yellow, although it would appear white if observed from a spacecraft. At sunset, when the sunlight passes through a longer path in the atmosphere than at other hours, intermediate wavelengths are also scattered, leaving direct light from the sun enhanced in the longest visible wavelengths (red light) and making the sun appear red.

[4] This effect makes it hard to understand what someone is saying when they are standing around a corner, because the voice sounds muffled due to the loss of the higher frequencies.

圖 3.7-10（地球內部 Q 結構剖面圖）：

縱軸為深度（0–6371 km），橫軸為 Q_μ（剪切波品質因子）： - **地殼**：Q_μ 約 300–600。 - **軟流圈（約 80–220 km）**：Q_μ 降至最低值（~80–100），為全球衰減最強區域，對應部分熔融的軟流圈。 - **岩石圈（Lid）**：Q_μ 高（> 600），冷而剛性。 - **下部地函**：Q_μ 平滑上升至 500 以上。 - **外核**：P 波 $Q_K \to \infty$（無衰減，理想液體）。 - **內核**：Q_μ 再次降低至約 150–300，反映高溫接近熔點。 此圖清楚展示 Q 結構與地球熱力學狀態的對應。

Q20. 解釋圖 3.7-18

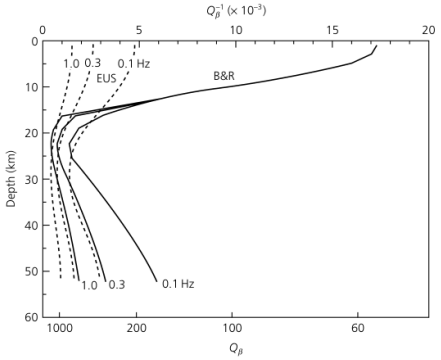

Fig. 3.7-17 Variation in attenuation with lithospheric depth for the eastern USA (EUS) and Basin and Range (B&R). Lower attenuation occurs for higher frequencies. (Mitchell, 1995. *Rev. Geophys.*, *33*, 441–62, copyright by the American Geophysical Union.)

Regional variations in crustal Q are often studied with *Lg* waves, a superposition of higher-mode surface waves that give prominent arrivals in continental regions. Q_{Lg} for the USA varies regionally (Fig. 3.7-18), with values as high as 750 in the stable East and as low as 250 in the tectonically active West. This regional difference in attenuation, also seen in Figs 3.7-1 and 3.7-17, has implications for seismic hazards (Section 1.2.2). Similarly, the fact that the USA tested nuclear weapons in the western USA, which is more attenuative than the areas used by the Soviet Union, is significant for verifying test ban treaties (Section 1.2.8).

Attenuation in the upper mantle varies with depth, with the lowest Q in the asthenosphere from about 80 to 220 km depth (Fig. 3.7-19). At these depths the temperature approaches, and perhaps exceeds, the melting temperatures of rock, so a small percentage of partial melt may exist. This pattern of attenuation is similar to that for seismic velocities, which are lowest in the asthenosphere. Hence both the elastic velocity and anelastic attenuation reflect the physical processes causing the mechanically weak asthenosphere. Beneath the asthenosphere, Q increases gradually with depth, presumably because temperature increases at a slower rate than pressure.

Q_μ increases with depth through the lower mantle, reaching values in excess of 500. There is some indication that attenuation is enhanced in the D″ region at the base of the mantle. Although no attenuation of *P* waves is detected for the outer core, there is significant attenuation of *PKIKP* waves traversing the inner core, yielding Q_K estimates in the range of 150–300.

Lateral variations in attenuation are studied using tomographic methods similar to those used for velocity (Sections 2.8.3, 7.3). Where temperatures vary over short distances, significant attenuation variations can occur, as shown in Fig. 3.7-3 for a mid-ocean ridge. Similarly, a cross-section through the back-arc spreading center above the Tonga subduction zone (Fig. 3.7-20) shows that Q_α exceeds 10,000 within the cold and rigid subducting slab, but is less than 75 beneath the hot back-arc basin. Such attenuation data, especially when combined with velocity data, are valuable for tectonic studies.

3.8 Composition of the mantle and the core

Seismology yields information about velocities within the earth. To derive inferences about the composition of the earth, the seismological data are combined with results from geology, geodesy, geomagnetism, cosmochemistry, and the physics and

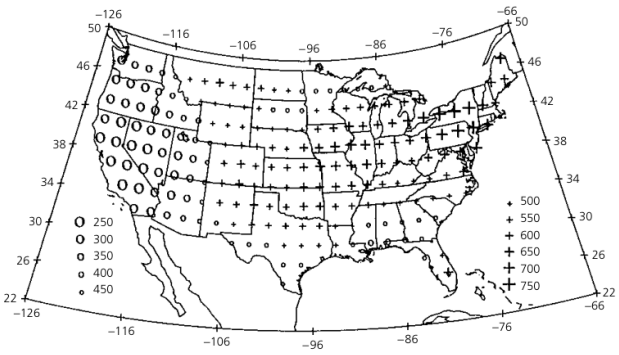

Fig. 3.7-18 Q_{Lg} for the USA mapped from the codas of 1 Hz *Lg* waves. Q_{Lg}, which reflects attenuation within the crust, shows higher attenuation in the tectonically active western USA and lower attenuation in the tectonically inactive east. (Mitchell *et al.*, 1997.)

圖 3.7-18（橫向衰減變化：湯加隱沒帶剖面圖）：

展示西太平洋湯加（Tonga）隱沒帶的 Q_α（P 波品質因子）橫向變化的二維剖面： - **隱沒冷板片**（藍色/高 Q 區）：$Q_\alpha > 10{,}000$，幾乎不衰減，因板片溫度低、剛性強。 - **弧後盆地（Back-arc Basin）**（紅色/低 Q 區）：$Q_\alpha < 75$，衰減極強，對應高溫地函楔（mantle wedge）及可能的部分熔融。 - **火山弧下方**：Q_α 最低，與岩漿房及高溫上湧地函對應。 此圖是衰減層析成像（attenuation tomography）的代表性成果，展現 Q 對溫度的高敏感性，遠優於速度層析成像對熱異常的解析能力。

附：線上互動報告

本報告互動版本與完整 PDF 下載已部署至 Hugging Face Space：
https://huggingface.co/spaces/Sam0424/seismic_ch3